Superplastic behavior of an Al–Mg alloy at elevated temperatures

R. Kaibyshev [a,*], F. Musin [a], D.R. Lesuer [b], T.G. Nieh [b]

[a] *Institute for Metals Superplasticity Problems, Khalturina Street 39, Ufa 450001, Russia*
[b] *Lawrence Livermore National Laboratory, L-342, PO Box 808, Livermore, CA 94551, USA*

Abstract

The superplastic properties and microstructural evolution of a 0.2% Zr and 1.6% Mn modified 5083 aluminum alloy with an initial grain size of 6.2 μm were examined at strain rates ranging from 10^{-5} to 10^{-1} s^{-1} in the temperature interval 500–580 °C. The maximum elongation-to-failure of 1150% was found at 570 °C, which is near the solidus temperature of 572 °C, and an initial strain rate of 2.8×10^{-3} s^{-1}. The corresponding strain rate sensitivity coefficient, m, was about 0.6. It was shown that increasing the temperature from 550 to 570 °C results in reduced cavitation and expanding the optimal interval of superplasticity toward lower strain rates due to the disappearance of the threshold stress. The influence of temperature on the mechanisms of superplastic deformation is discussed.

Keywords: Aluminum alloy; Superplasticity; Microstrutural evolution; Grain boundary sliding; Threshold stress

1. Introduction

The 5083 aluminum alloy (Al–4.7%Mg–0.7%Mn) has a great potential for aircraft and automotive body sheet applications due to its excellent combination of strength, corrosion resistance, weldability and low cost. In general, Al–Mg alloys with coarse-grained structure deform by viscous dislocation glide and exhibit an elongation-to-failure of about 240% with the coefficient of strain rate sensitivity $m = 0.3$ [1–4]. To further enhance superplastic properties, a stable, fine-grained ($\sim$5–10 μm) structure has been produced in these alloys via thermo-mechanical processing (TMP) [3,5–7]. Tensile ductility of about 500% was reported for the 5083 alloy with a fine-grained structure ($m \sim 0.5$) [3,7,8]. Superplasticity in fine-grained 5083 alloy is limited primarily by significant grain growth during superplastic deformation [9–11].

It is known that superplasticity in aluminum alloys is strongly dependent not only on grain size, but also on grain stability and cavitation [1,12]. In Al–Mg alloys, minor alloying additions of transition elements can enhance grain stability during superplastic deformation [5–7]. For example, Lavender et al. [6] showed that a modified 5083 alloy (Al–4.7%Mg–1.6%Mn–0.2%Zr) containing an increased amount of Al_6Mn particles and fine Al_3Zr precipitates was superplastic at a strain rate as high as $\dot{\varepsilon} = 10^{-2}$ s^{-1}. No cavitation was observed even after deformation to a strain of 1.1 at $\dot{\varepsilon} = 10^{-3}$ s^{-1} and 550 °C. Recently, Nieh et al. [13] also demonstrated that a minor addition of Sc (0.3%) produced high strain rate superplasticity in an Al–6%Mg alloy and suppressed cavitation. It is expected, therefore, that a highly stable grain structure produced by TMP may increase the temperature range in which superplasticity is observed. Recently, it was shown that increased tensile elongation could be attained in aluminum alloys near the solidus temperature [14,15]. However, superplastic behavior of Al–Mg has not been reported yet at such high temperatures.

* Corresponding author. Tel./fax: +7-3472-253856
E-mail address: rustam@anrb.ru (R. Kaibyshev).

Thus, the main purpose of the present work is to report superplastic behavior of a 0.2% Zr and 1.6% Mn modified 5083 aluminum alloy at elevated temperatures. Special attention will be given to microstructural evolution and cavitation behavior of the 5083 alloy during superplastic deformation.

2. Experimental

An experimental version of the 5083 alloy with a chemical composition of Al–4.7%Mg–1.6%Mn–0.2%Zr–0.18%Cr–0.1%Fe (in wt.%) was manufactured at the Kaiser Aluminum-Center for Technology by direct chill casting and then homogenization at 520 °C for 10 h.

The dispersoid-forming elements Mn and Zr were added to the alloy for grain refinement.

To develop a fine grained structure, a two-step TMP was applied.

i) The 5083Al was rolled at 400 °C with a reduction of 60%, followed by recrystallization annealing at 525 °C in a salt bath for 30 min.
ii) Next, the alloy was cold rolled with a reduction of 80%, followed by recrystallization annealing at 525 °C in a salt bath for 30 min.

The final thickness of the sheet produced via this TMP route was ~1.2 mm. Tensile samples with a 20 mm gauge length and 5 mm width were machined directly from these sheets; the loading axis was parallel to the rolling direction. Tensile tests were performed at temperatures ranging from 500 to 580 °C and strain rates ranging from 7×10^{-6} to 7×10^{-2} s^{-1}. An Instron universal testing machine (Model 1185) equipped with a three-zone split furnace was used. Temperature accuracy was within ±2 °C. The values of the strain rate sensitivity $m = \partial(\lg \sigma)/\partial(\lg \dot{\varepsilon})$ were determined by strain-rate-jump tests [12].

For optical metallography, the alloy was annealed at a temperature of 180 °C for 8 h in order to decorate grain boundaries with Al_3Mg_2 particles. These grain-boundary particles were revealed by etching with Hervenkel Reagent at 50 °C for 20 s. Metallographic analysis was carried out using a Neophot-32 microscope and an Epiquant automated image analyzer. Sections taken from planes containing the longitudinal (tension) and transverse directions were analyzed.

Differential thermal analysis was performed on a ~44 mg specimen during heating to 610 °C at a rate of 10 °C min^{-1} by using a Rigaku analyzer (Model Thermoflex).

For TEM examinations, samples were cut from the gauge section of tested tensile specimens and thinned to about 0.25 mm. Discs with a 3 mm diameter were electropolished to perforation with a Tenupol-3 twinjet polishing unit using a 200 ml CH_3COOH+150 ml H_3PO_4+100 ml HNO_3+50 ml H_2O solution at 6 V and 10 °C. The thin foils were examined using a JEOL-2000EX TEM with a double-tilt stage at an accelerating potential of 200 kV. The density of lattice dislocations was estimated using the intercept relationship [4,16]:

$$\rho = \frac{1}{t}\left(\frac{n_1}{L_1} + \frac{n_2}{L_2}\right), \quad (1)$$

where n_1 and n_2 are the numbers of intercepts on sets of orthogonal lines of total lengths L_1 and L_2 on the normal image, and t is the foil thickness, which was evaluated analyzing grain boundary extinction contours [16]. Energy dispersive X-ray analysis (EDS) of thin foils was carried out to identify second-phase particles by using an Oxford analytical attachment (Model Energy TEM200-INCA) to the JEOL-2000EX transmission electron microscope (TEM) operating at 200 kV. The analysis was done with a focused beam having a diameter of 100 nm, which was positioned on selected dispersoids.

For surface examination, specimens were mechanically polished and treated with boric acid to prevent oxidation. The specimens were deformed to true strains of 0.2 and 0.7 at a strain rate of 2.8×10^{-3} s^{-1} and temperatures of 525 and 570 °C. A JSM-840 scanning electron microscope was used to observe the surface features. Cavitation was measured on the as-polished and unetched samples, using the standard point-counting technique [5].

3. Experimental results

3.1. Differential thermal analysis

Fig. 1 shows a DTA curve for the modified 5083 aluminum alloy. Macroscopic melting of the 5083

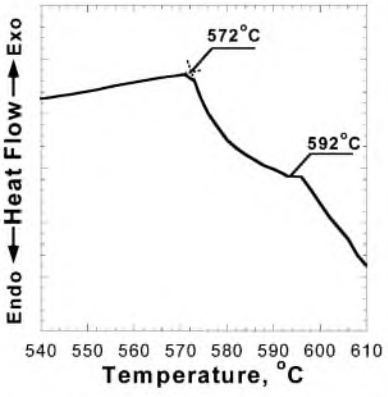

Fig. 1. DTA curve for the 5083 alloy. The solidus temperature (572 °C) and a temperature of 592 °C, at which extensive melting of the material starts, are indicated.

aluminum starts at 572 °C, which is the solidus temperature for this alloy. Therefore, the solidus temperature is 3 °C less than that of the 5083 alloy with standard chemical composition [3,17]. It is apparent that the reduced solidus temperature can be caused by a progressive dissolution of Mn with increasing temperature [17]. This dissolution may result in a weak exothermic reaction in the temperature range 550–572 °C followed by an endothermic reaction associated with melting (Fig. 1). Extensive melting takes place at temperatures above 592 °C. The liquidus temperature of the commercial 5083 alloy is about 633 °C [17].

3.2. Microstructure before deformation

The two-step TMP resulted in a uniform grain structure with an average grain size of 6.2 μm. The grains were equiaxed (Fig. 2a). Second-phase particles were identified using EDS analysis (Fig. 2b). Fig. 2c represents a typical EDS spectrum obtained from

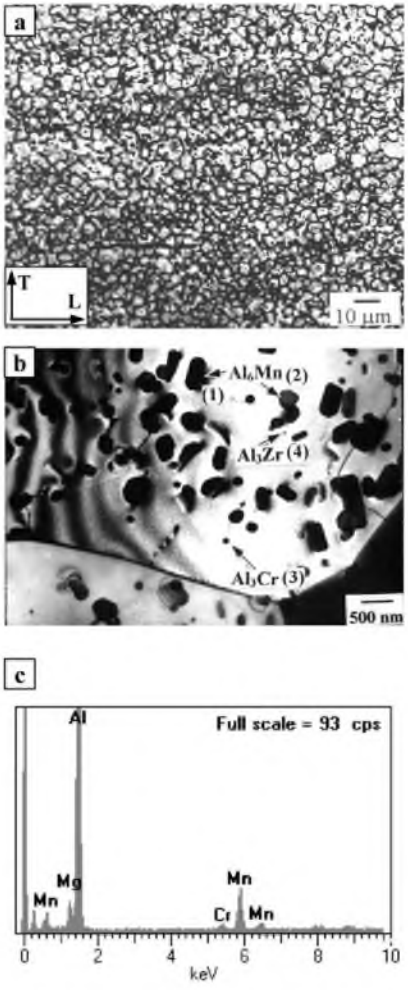

Fig. 2. Initial microstructure of the 5083 alloy after the TMP: (a) optical metallograph, arrows indicate the longitudinal (rolling) (L) and transverse (T) directions; (b) TEM, (c) energy dispersion X-ray spectrum for a dispersoid indicated as 1.

Table 1
Elemental composition in weight (first number) and atomic% (second number) for the dispersoids indicated in Fig. 2b

Dispersoid number	Al	Mn	Cr	Zr
1	83.5/91.4	12.1/6.5	1/0.6	0.2/0.07
2	91.1/83.1	14.9/8	1/0.6	0.93/0.3
3	88.4/94	3.9/2	6.7/3.7	1/0.3
4	86.8/94.3	3.1/1.7	0/0	4.3/1.4

particles exhibiting a plate-like morphology which were approximately 0.3 μm in longitudinal and 0.1 μm in transverse dimensions (Fig. 2b). The presence of manganese, as shown in Fig. 2c and Table 1, suggests that the nature of this particle is Al_6Mn. Essentially similar EDS spectra (Table 1) were obtained from the coarse particles exhibiting a polygonal shape (Fig. 2b). Such Al_6Mn particles are enriched by Cr and Zr. The spectrum taken from the dispersoid number 3 with equiaxed shape and an average size of 0.14 μm (Fig. 2b) indicates excess concentration of chromium (Table 1). Equiaxed particles with an average size of 30 nm are enriched with zirconium (Table 1). Therefore, it is apparent that the equiaxed particles with sizes 0.14 μm and 30 nm are Al_3Cr and Al_3Zr phases, respectively. Notably, enhanced concentrations of Zr and Mn were found at selected points on 0.14 μm particles of Al_3Cr (Table 1).

The density of lattice dislocations was measured to be about 10^{12} m^{-2} after the TMP and was less than 3×10^{10} m^{-2} after annealing at 570 °C for 1800 s.

3.3. Mechanical properties

The true stress–true strain curves for the 5083 alloy at an initial strain rate of 2.8×10^{-3} s^{-1} and temperatures ranging from 500 to 580 °C, and at 570 °C and strain rates ranging from 1.4×10^{-4} to 7×10^{-2} s^{-1} are presented in Fig. 3a and b, respectively. Extensive strain hardening takes place initially. After reaching a maximum stress, the flow stress continuously decreases until fracture. A well defined peak in flow stress can be observed, and no steady-state flow occurs (Fig. 3). Increasing temperature or decreasing strain rate leads to a reduction in the strain-hardening coefficient and a shift of the peak stress to a higher strain (Fig. 3). For example, at temperatures of 525 and 570 °C, the peak stresses were found at strains of 1 and 1.6, respectively. At 580 °C, the softening stage was never reached because of reduced plasticity.

The flow stress (at a strain of 0.34) as a function of strain rate is plotted on a double-logarithmic scale in Fig. 4a. Three regions of superplastic deformation can be identified. The maximum values of elongation-to-failure, δ, and the coefficient of strain rate sensitivity,

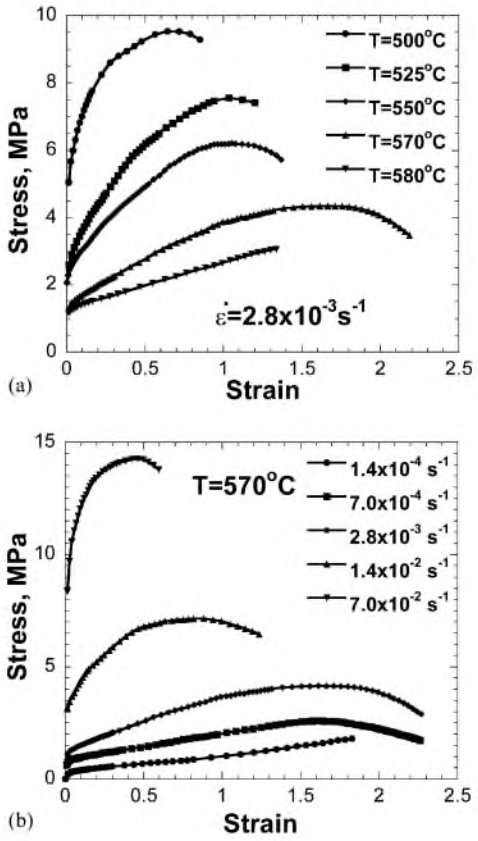

Fig. 3. Effect of temperature (a) and strain rate (b) on the true stress–true strain curves for the modified 5083 alloy.

m, are found to occur in the second region (where $m \geq 0.33$ and $\delta \geq 300\%$) and tend to decrease on either side of the strain rate associated with these maximum values (Fig. 4b and c). The optimal strain rate region for superplasticity (region 2) tends to expand with increasing temperature from 550 to 570 °C. The strain rate ranges for superplasticity (distinguished by $m \geq 0.33$) are from 7×10^{-4} to 1.6×10^{-2} s^{-1} at 550 °C, and from 2.8×10^{-5} to 1.6×10^{-2} s^{-1} at 570 °C. At 550 °C, the highest value of elongation-to-failure (600%) is observed at $\dot{\varepsilon} = 7 \times 10^{-4}$ s^{-1} and remains almost unchanged at lower strain rates. The maximum m value of 0.5 occurs at strain rates ranging from 2.8×10^{-3} to 7×10^{-3} s^{-1}. At 570 °C, a well-defined maximum in elongation-to-failure (1150%) is observed at $\dot{\varepsilon} = 2.8 \times 10^{-3}$ s^{-1} while the highest m value of 0.6 occurs at $\dot{\varepsilon} = 1.4 \times 10^{-3}$ s^{-1}. At this temperature, region 1 was found only at strain rates less than 10^{-5} s^{-1}. It is worth noting that the m value tends to decrease with strain during superplastic deformation at all temperatures examined (Fig. 5).

The flow stress decreases monotonically with increasing temperature, and the m value and the elongation-to-failure tend to increase in the temperature interval 500–570 °C (Fig. 6). The peak of the elongation-to-failure is observed at 570 °C. Higher temperatures result in

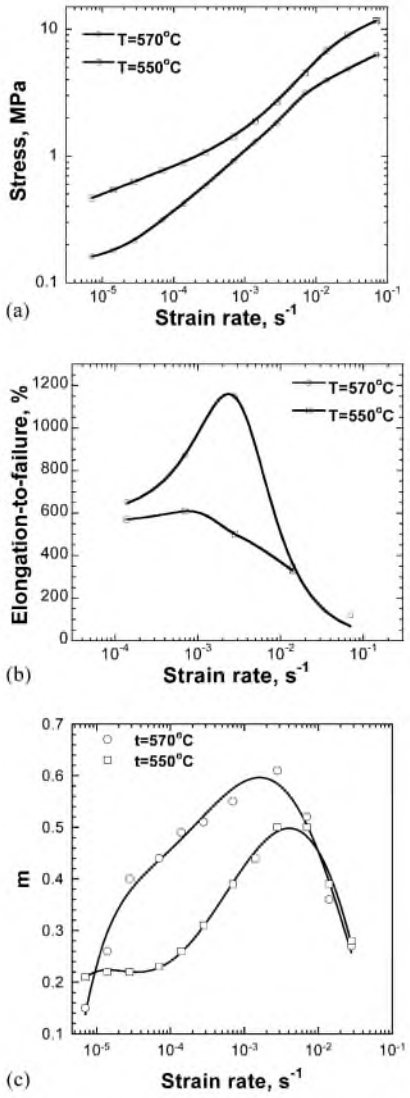

Fig. 4. The variation of flow stress (a), elongation-to-failure (b) and the coefficient of strain rate sensitivity, m, (c) with strain rate.

decreases in both m and δ values and a shift of the

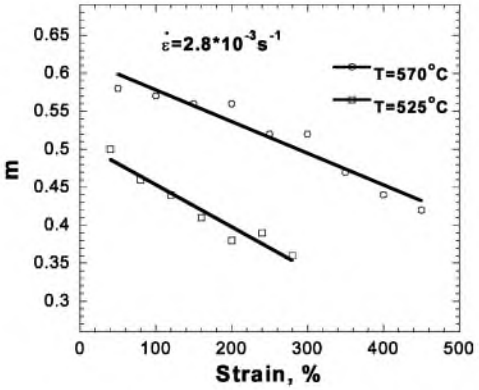

Fig. 5. Typical dependencies for the variation of the coefficient of strain rate sensitivity, m, with strain at $\dot{\varepsilon} = 2.8 \times 10^{-3}$ s^{-1}.

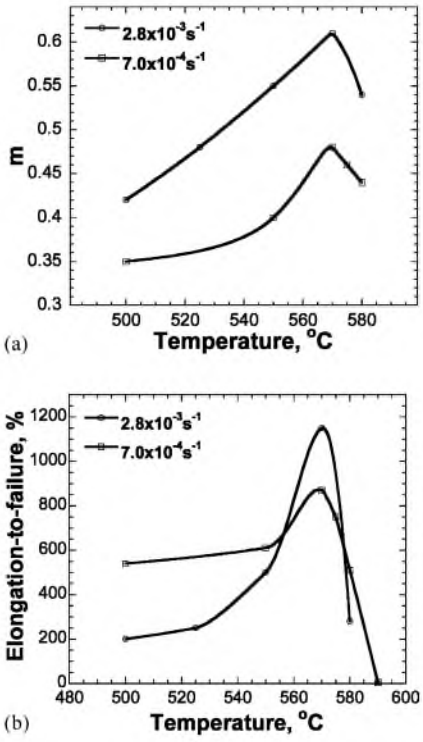

Fig. 6. The variation of the coefficient of strain rate sensitivity (a) and elongation-to-failure (b) with temperature.

highest value of elongation-to-failure to lower strain rates. At 580 °C, which is higher than the solidus temperature, the highest δ value is about 500% at $\dot{\varepsilon} = 7 \times 10^{-4}$ s^{-1} with a corresponding m value of about 0.44. At 590 °C, failure occurs with limited plastic flow. Since the solidus temperature is ~572 °C, this reduced ductility is apparently associated with the presence of massive liquid phase.

3.4. Microstructural evolution

3.4.1. Grain growth

Grain growth in the present modified 5083 Al occurs under both static and dynamic conditions at $T >$ 500 °C (Table 2). Compared with other grades of 5083Al [4,5,9,10,18], this alloy exhibits improved microstructural stability under static annealing and during superplastic flow. For instance, the static grain growth at 550 °C in the present 5083 alloy is at least half that reported previously [4,9,10,18] for other grades of 5083 alloy. Dynamic grain growth was also slower in the present 5083 alloy. Compared with commercial grades of the 5083 alloy [4,8], the rate of dynamic grain growth is slower by a factor of 3. Also, in comparison with Al–4.7%Mg–1.6%Mn [5] and Al–4.7%Mg–0.7%Mn–0.4%Cu alloys [18], the rate of dynamic growth is less by 20%. The slower static and dynamic grain growth rates can be attributed to the Zr and Mn additions.

Static annealing of the modified 5083 Al alloy prior to deformation produced equiaxed grains. However, significant grain elongation was observed during superplastic deformation (Table 2). The grain aspect ratio, defined as the ratio of the grain dimension in the longitudinal direction to that in the transverse direction, reaches a maximum at 550 °C and tends to decrease with increasing temperature up to 570 °C. It is of interest to note that, for other grades of 5083 alloy, equiaxed grains continuously elongate along the tension axis during superplastic deformation because of dislocation creep [9,18]. In the present 5083 alloy, the grain aspect ratio is slightly less after deformation at $T =$ 550 °C and $\dot{\varepsilon} = 2.8 \times 10^{-3}$ s^{-1} in comparison with other grades of 5083Al [9,18], which is indicative of the decreased contribution of dislocation glide to total elongation in the modified 5083Al [11,18]. Therefore, the increased plasticity at 570 °C in comparison with 550 °C can be associated with the increased contribution of grain boundary sliding (GBS) to total deformation. Both concurrent grain growth and an increasing grain aspect ratio with strain during superplastic deformation are expected to reduce the likelihood of GBS and thus superplastic elongation. This results in a gradual reduction in the m value with increasing strain (Fig. 5).

3.4.2. Dislocation structure

Dislocation microstructures were examined in samples strained to $\varepsilon = 1.2$ at $\dot{\varepsilon} = 2.8 \times 10^{-3}$ s^{-1} and two different temperatures (Fig. 7). At 525 °C, the average density of lattice dislocations was about 5×10^{12} m^{-2} (Fig. 7a). At 570 °C, the density of lattice dislocation was ~10^{10} m^{-2} (Fig. 7b). Therefore, the lattice

Table 2
Average grain size (μm) after static (grip section) and dynamic (gauge section) annealing at different temperatures and $\dot{\varepsilon} = 2.8 \times 10^{-3}$ s^{-1}

	500 °C	525 °C	550 °C	570 °C	580 °C
Annealing time (s)	2700	2880	3900	6600	3000
True strain	1.1	1.25	1.8	2.5	1.3
Grip	6.2±0.5	7.1±0.3	9.4±0.4	10.5±0.4	12.5±0.5
Gauge (longitudinal)	13.7±0.5	15.5±0.6	22.5±0.9	24.0±0.9	24.8±1.0
Gauge (transverse)	8.6±0.3	8.7±0.3	11.8±0.5	13.6±0.5	15±.06
Grain aspect ratio	1.59	1.78	1.91	1.76	1.65

The time of static annealing in the grip section (in s) and the true strain in the gauge section are indicated.

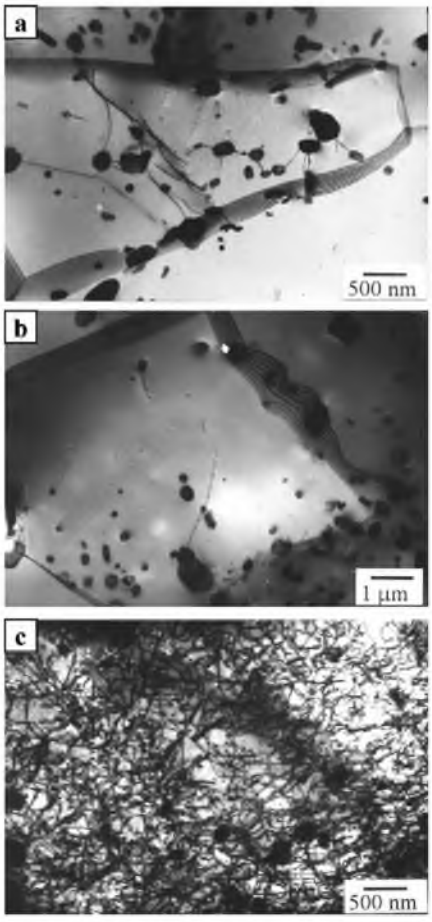

Fig. 7. Dislocation structure at $\dot{\varepsilon} = 2.8 \times 10^{-3} s^{-1}$ and $\varepsilon = 1.2$; (a) $T =$ 525 °C; (b, c) $T = 570$ °C.

dislocation density observed after superplastic deformation is very similar to that observed after static annealing. Dislocations generated during superplastic deformation inside grains are continuously annihilated by recovery processes. On the other hand, extensive particle-dislocation interactions were observed in the superplastically deformed sample (Fig. 7a). Despite this interaction, the average dislocation density in the present 5083 alloy is still about one order of magnitude less than that in the conventional 5083 alloy [4,10]. Apparently, the drag effect of dispersoids on mobile dislocations does not influence the density of lattice dislocations within grain interiors. It is apparent that the dislocation density is controlled by the rate of dislocation absorption by grain boundaries [12]. An increase in the test temperature from 525 to 570 °C enhances the capacity of grain boundaries to adsorb dislocations [12]. Mobile lattice dislocations can be rapidly adsorbed by the boundaries of fine grains during GBS. This is supported by the fact that at 570 °C, a higher lattice dislocation density ($\rho \sim 10^{13}$ m^{-2}) was observed in larger grains (Fig. 7c), in which extensive GBS did not occur [12].

3.4.3. Cavitation

To measure cavitation during superplastic deformation, specimens deformed to failure at $\dot{\varepsilon} = 2.8 \times 10^{-3}$ s^{-1} and different temperatures were examined metallographically. Areas within 5 mm of the fracture surface (Table 3, Fig. 8) were analyzed. At $T < 570$ °C, small cavities with irregular shapes developed along the tensile direction (Fig. 8a and b). With continuing deformation, these cavities coalesced in the tensile direction, which resulted in significant cavity growth. No cavity interlinkage was observed in the transverse direction. These observations suggest a plasticity-controlled cavity growth mechanism [2], indicating cavitation is a result of extensive GBS [1,2,19]. Notice that the area fraction of cavities increases from 1.8 to 6.5% as the temperature increases from 500 to 550 °C, but decreases at higher temperatures. At 570 °C, fine, equiaxed cavities dominate. At 580 °C, cavities are practically equiaxed (Fig. 8c). These results suggest that diffusion-controlled cavity growth dominates at $T \geq 570$ °C. Plasticity-controlled cavity growth was suppressed in this high temperature range.

3.4.4. Grain boundary sliding

Surface observations showed that GBS plays an important role in superplastic deformation at all testing temperatures, and the uniformity of GBS tends to increase with increasing temperature (Fig. 9). At 525 °C, non-uniform GBS occurs in a cooperative manner through the shift of grain groups as a unit relative to each other along common grain boundary surfaces [19]. The average size of these grain groups after $\varepsilon = 0.2$ is ~ 4–6 units of the average matrix grain size (Fig. 9a). At 570 °C, GBS is essentially uniform and the sliding of individual grains dominates even after $\varepsilon = 0.2$ (Fig. 9b). Increasing strain leads to the operation of GBS in an individual manner (Fig. 9c). Thus, increasing the temperature from 525 to 570 °C leads to transition from the sliding of grain groups to the sliding of individual grains.

4. Discussion

The addition of Zr and Mn to the 5083Al alloy result in the formation of Al_3Zr-type dispersoids and an increased volume fraction of Al_6Mn-particles. These particles effectively pin grain boundaries and improve grain stability of the modified 5083 alloy during static annealing and under superplastic deformation conditions. As a result, superplasticity in this alloy shifts toward higher strain rates by about one order of magnitude, as compared with commercial grades of the 5083 alloy [3,4,6,7]. Also, as a result of the stable microstructure, the modified 5083 alloy exhibits excellent superplastic properties at 570 °C, which is slightly

Table 3
Cavitation (area fraction%) in the gauge section ($\dot{\varepsilon} = 2.8 \times 10^{-3}\ s^{-1}$)

	500 °C	525 °C	550 °C	570 °C	580 °C
Longitudinal	1.8±0.07	2.1±0.08	6.5±0.26	3.0±0.12	0.5±0.02
Transverse	1.5±0.06	1.7±0.07	5.0±0.2	1.8±0.07	0.5±0.02
Elongation (%)	200	290	500	1150	280

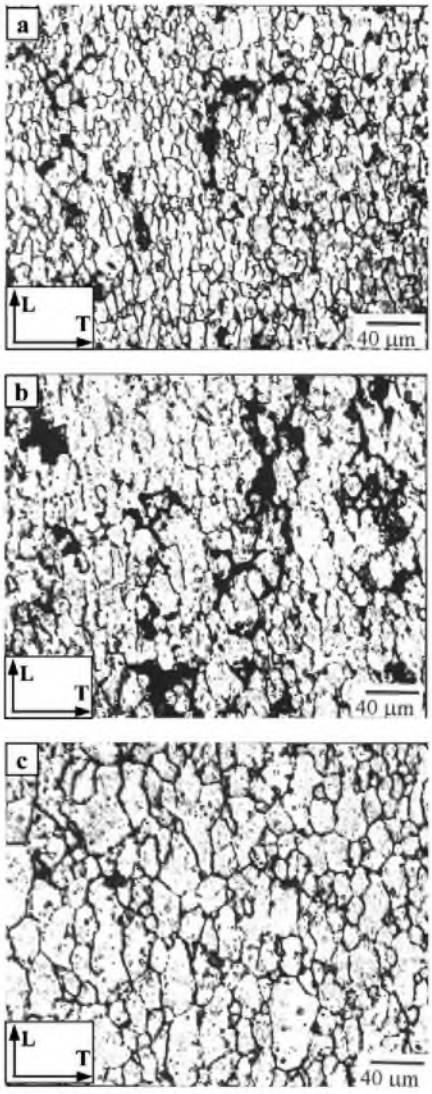

Fig. 8. Optical micrographs of samples deformed to failure at $\dot{\varepsilon} = 2.8 \times 10^{-3} s^{-1}$: (a) 525 °C, (b) 550 °C and (c) 580 °C. Micrographs were taken 5 mm from fracture surface. Arrows indicate the longitudinal (tension) (L) and transverse (T) directions.

below the solidus temperature. In comparison, commercial 5083 Al has only moderate tensile ductility at this high temperature [3,4].

It is noted that the largest superplastic elongation was observed below the solidus temperature. Thus, the presence of a liquid phase was unlikely to be responsible for the enhanced tensile ductility. This is indirectly supported by the fact that the optimal region of superplastic deformation (region 2) extends to low strain rates at 570 °C. This phenomenon has also been observed in high-purity superplastic eutectoid alloys [20–22] and can be associated with the disappearance of a threshold stress at 570 °C.

It has been suggested [1,20–22] that threshold behavior in superplastic materials is associated with an interaction between impurity atoms segregated at boundaries and grain boundary dislocations. To calculate the threshold stress, the peak stresses and corresponding strain rates were used with the assumption that steady-state flow is represented by the peak stress [23,24]. Standard procedures were used to determine the threshold stress (σ_{th}) from the step-strain-rate tests [23–25]. Specimens were strained to the peak stress, then the strain rate was suddenly changed. The experimental data from region 1 and region 2 of superplastic deformation were plotted as $\dot{\varepsilon}^{1/n}$ versus steady state flow stress, σ, on a double-linear scale at different temperatures. Data in the strain rate interval were best fitted to a straight line by varying the n values. The intercepts to the stress axis yield the σth values, which, in principle, are independent of the applied stresses. Variation in the values of n provided the best linear fit with $n = 2$. The values of threshold stress obtained are listed in Table 4. It is seen that in the temperature range 500–550 °C there exists a temperature dependence of the threshold stress (Fig. 10) which obeys the equation [20–25]:

$$\frac{\sigma \mathrm{th}}{G} = B_o \exp\left(\frac{Q_o}{RT}\right), \tag{2}$$

where B_o is a constant, and Q_o is an energy term. The value $Q_o = 60$ kJ mol^{-1} was obtained by plotting ln σth/G versus $1/T$ in the temperature interval 500–550 °C. At $T = 570$ °C, no threshold stress was found.

Thus, the superplastic, modified 5083 alloy exhibits threshold behavior at temperatures ranging from 500 to 550 °C and behaves like a typical high-purity superplastic alloy [20–22] at the elevated temperature 570 °C. The absence of threshold stress results in the extension of superplasticity to lower strain rates at this temperature as compared with that at 550 °C (Fig. 4) [20–22]. In fact, at 570 °C, region 1 almost disappears.

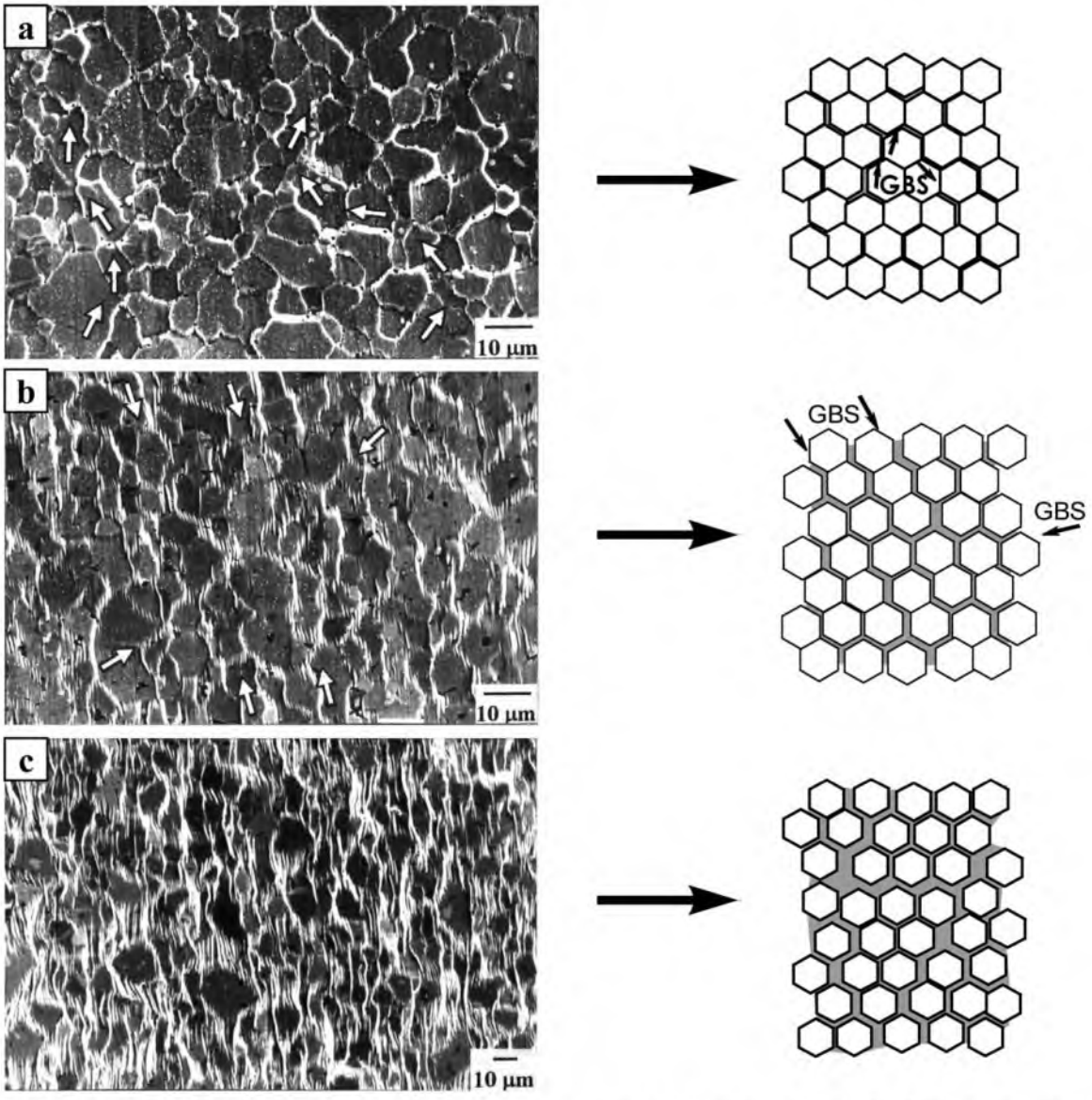

Fig. 9. Surface observations after superplastic deformation and schematic illustration of GBS at $\dot{\varepsilon} = 2.8 \times 10^{-3}\ s^{-1}$: (a) $T = 525\ ^{\circ}C$, $\varepsilon = 0.2$; (b) $T = 570\ ^{\circ}C$, $\varepsilon = 0.2$ and (c) $T = 570\ ^{\circ}C$, $\varepsilon = 0.7$. Arrows indicate non-uniform GBS along common grain boundaries.

Table 4
Threshold stress σ_{th} at different temperatures

	500 °C	525 °C	550 °C	570 °C
σth (Mpa)	2.2	1.5	1.2	0

At $T \leq 550\ ^{\circ}C$, GBS occurs along favorably oriented grain boundary surfaces. The break away of grain boundary dislocations can occur under an applied stress, which is higher than the threshold stress. The maximum stress is attained along grain boundary surfaces which are located at about a 45° angle. As a result, cooperative GBS occurs along common boundaries with the maximum values of Schmid factor. At 570 °C, the disap-

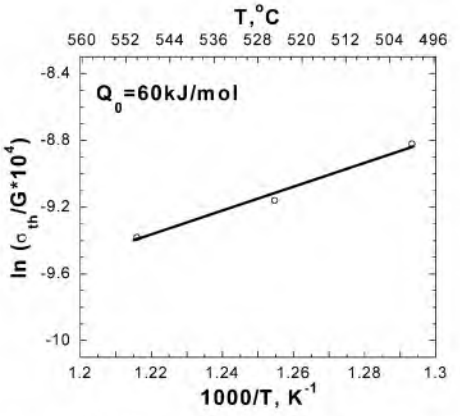

Fig. 10. Temperature dependence of the modulus-normalized threshold stress.

pearance of the threshold stress, suggests that the grain boundary dislocations can break away from impurities due to thermal activation. It seems that this detachment is a necessary condition for a high rate of dislocation adsorption by grain boundaries and, therefore, GBS [12]. The sliding of individual grains can occur along boundaries oriented at different angles to the tension axis, since no threshold stress exists. Highly uniform GBS takes place. As a result, the accommodation of GBS by dislocation glide occurs easily, and plasticity-controlled cavity growth, which can be associated with non-accommodated GBS [2], is suppressed. Therefore, reduced cavitation during superplastic deformation and enhanced ductility at elevated temperature are a consequence of increased uniformity of GBS.

At 580 °C, which is higher than the solidus temperature, the present 5083 alloy also exhibits satisfactory superplastic properties. These results are in contrast to the decrease in ductility observed in an Al–5%Mg alloy with a coarse grain structure [26]. The results suggest that Al–Mg alloys with a stable, fine grain structure can exhibit superplastic behavior in the semi-solid state.

5. Conclusions

A 0.2% Zr and 1.6% Mn modified 5083 alloy can be thermomechanically processed into a uniform fine-grained (6.2 μm) microstructure. This alloy has improved grain stability under both static and dynamic annealing conditions, as compared with conventional 5083 Al. The modified 5083 alloy exhibits superplastic behavior in the temperature range of 500–570 °C. Superior superplastic properties, with a maximum elongation-to-failure of 1150%, occur at a strain rate of 2.8×10^{-3} s^{-1} and 570 °C, which is slightly below the solidus temperature. At this temperature, the 5083 Al behaves like a typical high-purity superplastic alloy. Increasing the temperature from 550 to 570 °C results in an expansion of the strain rate range for superplasticity (where $m \geq 0.33$), from 7×10^{-4}–1.6×10^{-2} s^{-1} to 2.8×10^{-5}–1.6×10^{-2} s^{-1}. This extension in strain rate range is caused by the disappearance of the threshold behavior at 570 °C. Decreased cavitation and dislocation density, and increased uniformity of GBS were observed at 570 °C in comparison with that at lower temperatures.

Acknowledgements

This work was performed under the auspices of the US Department of Energy under contract No. W-7405-ENG-48.

References

[1] T.G. Nieh, J. Wadsworth, O.D. Sherby, Superplasticity in Metals and Ceramics, Cambridge University Press, New York, 1996, p. 210.
[2] J. Cadek, Creep of Metallic Materials(in Russian), Mir, Moscow, 1987, p. 304.
[3] R. Verma, A.K. Ghosh, S. Kim, C. Kim, Mater. Sci. Eng. A191 (1995) 143.
[4] F. Li, W.T. Roberts, P.S. Bate, Acta Mater. 44 (1996) 217.
[5] K. Kannan, C.H. Jonson, C.H. Hamilton, Metall. Mater. Trans. 29A (1998) 1211.
[6] C.A. Lavender, J.S. Vetrano, M.T. Smith, S.M. Bruemmer, C.H. Hamilton, Scr. Metall. Mater. 30 (1994) 565.
[7] A.O. Nikiforov, V.I. Polkin, I.I. Novikov, Non-Ferrous Metals 3 (1995) 54(in Russian).
[8] C.F. Martin, J.J. Blandin, L. Salvo, Mater. Sci. Eng. A297 (2001) 212.
[9] P.A. Friedman, A.K. Ghosh, Metall. Trans. 27A (1996) 3827.
[10] F. Li, Mater. Sci. Tech. 13 (1997) 17.
[11] D.H. Bae, A.K. Ghosh, Acta Mater. 48 (2000) 1207.
[12] O.A. Kaibyshev, Superplasticity of Alloys, Intermetallides, and Ceramics, Springer-Verlag, Berlin, 1992, p. 316.
[13] T.G. Nieh, L.M. Hsiung, J. Wadsworth, R. Kaibyshev, Acta Mater. 46 (1998) 2789.
[14] J. Koike, K. Miki, K. Maruyama, H. Oikawa, Phil. Mag. A. 78 (1998) 599.
[15] K. Higashi, T.G. Nieh, M. Mabuchi, J. Wadsworth, Scr. Metall. Mater. 32 (1995) 1079.
[16] P.B. Hirsh, A. Howie, R.B. Nicholson, D.W. Pashley, M.J. Whelan, Electron Microscopy of Thin Crystals, Butterworths, London, 1965, p. 574.
[17] Kaiser Aluminum and Chemical Corporation, Center for Technology, Metallography Handbook for 5083Al, Pleasanton, CA, 1992, p.5.
[18] F. Li, D.H. Bae, A.K. Ghosh, Acta Mater. 45 (1997) 3887.
[19] M.G. Zelin, N.A. Krasilnikov, R.Z. Valiev, M.W. Grabski, H.S. Yang, A.K. Mukherjee, Acta Metall. Mater. 42 (1994) 119.
[20] P.K. Chaudhary, F.A. Mohamed, Acta Metall. 36 (1988) 1099.
[21] S. Yan, C. Eartman, F. Mohamed, Phil. Mag. A 69 (1994) 1039.
[22] K. Duong, F.A. Mohamed, Acta Mater. 46 (1998) 4571.
[23] Y. Li, S.R. Nutt, F. Mohamed, Acta Mater. 45 (1997) 2607.
[24] Y. Li, F.A. Mohamed, Acta Mater. 45 (1997) 4775.
[25] F.A. Mohamed, K.T. Park, E.J. Lavernia, Mater. Sci. Eng. A150 (1992) 21.
[26] H. Iwasaki, T. Mori, M. Mabuchi, K. Higashi, Acta Mater. 46 (1998) 6351.